Scientific Research Publishing

Advances in Chemical Engineering and Science, 2022, 12, 197-209
https://www.scirp.org/journal/aces
ISSN Online: 2160-0406
ISSN Print: 2160-0392

Practical Method for Designing Gas Conditions of Atomic Layer Deposition

Linsheng Xie[1], Hitoshi Habuka[1], Harunori Ushikawa[2]

[1]Yokohama National University, Yokohama, Japan
[2]Watty Corporation, Sagamihara, Japan
Email: habuka-hitoshi-ng@ynu.ac.jp

How to cite this paper: Xie, L.S., Habuka, H. and Ushikawa, H. (2022) Practical Method for Designing Gas Conditions of Atomic Layer Deposition. *Advances in Chemical Engineering and Science*, **12**, 197-209.
https://doi.org/10.4236/aces.2022.124014

Received: September 6, 2022
Accepted: October 14, 2022
Published: October 17, 2022

Copyright © 2022 by author(s) and Scientific Research Publishing Inc.
This work is licensed under the Creative Commons Attribution International License (CC BY 4.0).
http://creativecommons.org/licenses/by/4.0/

Open Access

Abstract

In order to effectively develop the atomic layer deposition (ALD) reactor and process, having huge potentials and applications in the advanced technology fields, a practical design method of the gas conditions for the ALD was studied using computational fluid dynamics (CFD). The design method consisting of the following four steps was studied. 1) At a low gas pressure producing no gas recirculation, the maximum difference in the gas phase temperature from the sample stage temperature, ΔT, was obtained at various chamber wall temperatures. 2) The ΔT value was studied at various gas pressures producing the gas recirculation. 3) For determining the applicable process conditions, contour diagrams of the temperature uniformity were obtained utilizing the temperature uniformity equations consisting of various process parameters. 4) The relationships of the maximum gas residence time with the gas flow rate and the gas pressure were obtained. The process in this study is expected to be practical for designing the thermal and gas flow conditions for achieving a fast ALD.

Keywords

Atomic Layer Deposition, Gas Temperature Uniformity, Gas Residence Time, Computational Fluid Dynamics

1. Introduction

Advanced electronic devices for information and various applications are based on the technique of fabricating significantly small and thin structures [1]. These applications require atomically thin flat films, which are produced by the atomic layer deposition (ALD) technique [1] [2] [3] [4].

While the ALD has a significant capacity to form a thin flat film, the deposi-

tion is quite slow. The slow deposition rate is caused by the self-limited mechanism and the process conditions in the reactor. The ALD productivity is considered to be improved by two measures [1] [2] [5]. 1) Many substrates can be loaded in the chamber when the gas phase temperature in the reactor is highly uniform. 2) The overall process time can be shorter when the previously-introduced precursor and the byproducts are quickly removed from the reactor prior to the introduction of the next precursor. These two measures are expected to be studied accounting for the temperature uniformity and the gas residence time in the reactor from the viewpoint of the transport phenomena based on computational fluid dynamics (CFD) [6].

There have been many notable CFD studies for the various ALD reactors and various processes [7]-[12] that analyzed the gas flow, temperature, and precursor transport, in detail. As the next step for easily and quickly designing and choosing the ALD process parameters, methods integrating the CFD results are expected.

In this study, the gas flow and the heat transport in the ALD reactor are evaluated by the CFD taking into account the various ALD process parameters. Based on the results, the practical design method of the ALD process conditions was studied by developing the equations and diagrams of the temperature uniformity with accounting for the behavior of the gas residence time.

2. Numerical Calculation

Figure 1 shows the geometry of the ALD reactor in this study. As shown in **Figure 1(a)**, there is a circular-shaped stage (507 mmΦ) and circular-shaped gas distributor (505 mmΦ) in the cylindrical-shaped chamber. The distance between the outside edge of stage and the inner surface of chamber wall is 4 mm. The gas distributor is placed 160 mm above the stage. The gas distributor has many pinholes for spreading the gas over the stage. The gas inlet was placed above the gas distributor. A quarter part of the reactor is taken into account for the numerical calculations assuming a periodic boundary condition.

As shown in **Figure 1(b)**, the cross-shaped small table made of stainless steel is placed at the center of the stage when the gas residence time is evaluated. The cross-shaped table is designed by crossing two pieces of the long table, the height, width and length of which are 80 mm, 58 mm and 137 mm, respectively.

The argon gas is introduced downward from the inlet at a uniform velocity over the inlet corresponding to the gas flow rate of 50 - 500 sccm, the temperature of 25˚C, and the pressure of 50 - 5000 Pa. The temperatures of the gas distributor, chamber wall and stage were 25˚C - 400˚C, 200˚C - 400˚C and 350˚C, respectively.

The numerical calculations based on fluid dynamics take into account the pressure, momenta and enthalpy equations using the Fluent software (Cybernet Systems Co., Ltd., Tokyo, Japan). The gas phase temperature profile was evaluated along with the vertical lines between the stage and the gas distributor at

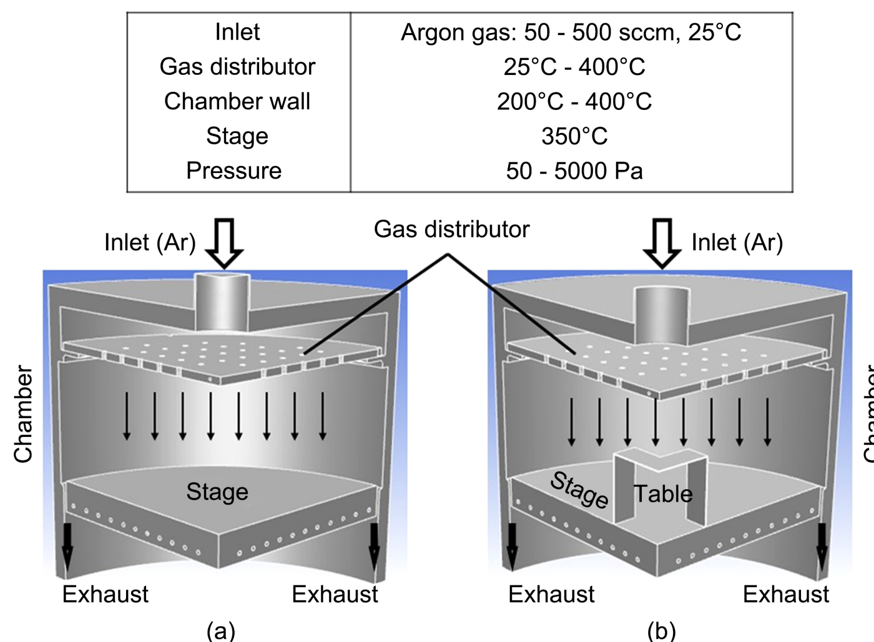

Figure 1. Geometry of ALD reactor, (a) without table and (b) with table.

the O, A, B and C positions which are 0, 125, 150 and 175 mm, respectively, from the center position of the stage. The influences of the various parameters on the temperature uniformity are expressed by the equations consisting of the process parameters. The maximum gas residence time was evaluated by tracing the virtual particles from the inlet to the exhaust.

3. Results and Discussion

3.1. Temperature without Gas Recirculation

The numerical calculations evaluated the influences of the chamber wall temperature and the gas pressure on the gas phase temperature and the gas flow. In order to individually evaluate the heat transport by the thermal conduction and that by the gas recirculation, the calculation was first performed at a sufficiently low pressure producing no gas recirculation.

Figure 2 shows the overall gas flow motion and the gas velocity distribution at the chamber wall temperatures of (a) 200˚C, (b) 300˚C, (c) 350˚C and (d) 400˚C. For these calculations, the argon gas was supplied from the inlet at the gas flow rate of 100 sccm, the temperature of 25˚C and the pressure of 50 Pa. The temperatures of the gas distributor and the stage were fixed at 350˚C.

Figure 2(a) shows the gas flow when the chamber wall temperature was 200˚C. The argon gas flows downward through the gas distributor. In the center region of the chamber, the gas flows down to the stage and changes its direction to the outside edge of the stage. In the region around a half radius of the gas distributor, the gas seems to go straight to the space between the stage and the chamber wall. The gas from the outside region of the gas distributor also goes straight and downward to the exhaust.

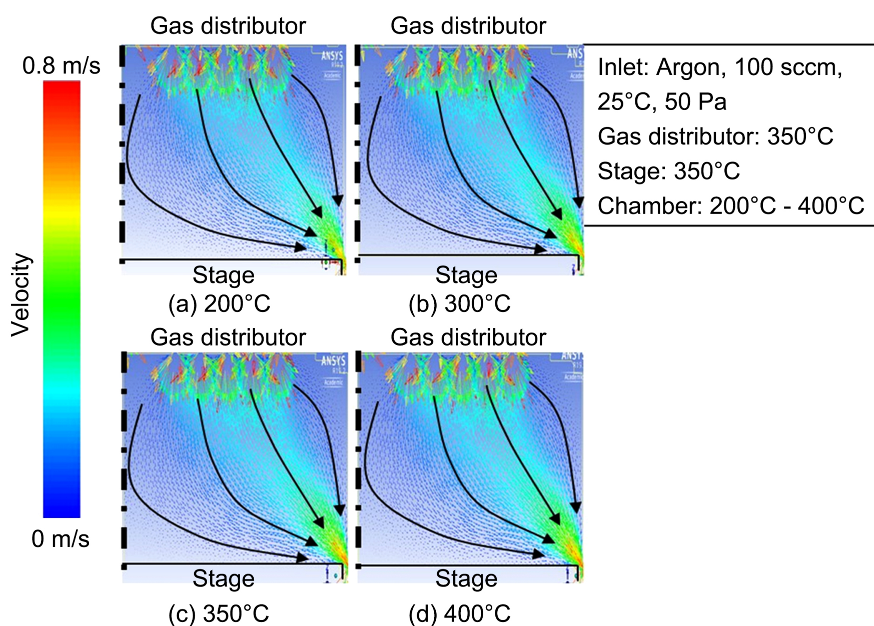

Figure 2. Gas flow and velocity at chamber wall temperature of (a) 200˚C, (b) 300˚C, (c) 350˚C and (d) 400˚C.

As shown in **Figure 2(b)**, **Figure 2(c)** and **Figure 2(d)** at the chamber wall temperatures of 300˚C, 350˚C and 400˚C, respectively, the gas flow directions are similar to those in **Figure 2(a)**. Overall, the gases flow without recirculation in the reactor at 50 Pa and 100 sccm in the temperature range between 200 and 400˚C.

During the gas flow without any gas recirculation, such as those in **Figure 2**, the heat is transported between various parts mainly by thermal conduction. Thus, the influence of the chamber wall temperature on the gas phase temperature can be clearly evaluated. **Figure 3** and **Figure 4** show the gas phase temperature distribution at the chamber wall temperatures of (a) 200˚C, (b) 300˚C, (c) 350˚C and (d) 400˚C. The gas flow rate, gas temperature and pressure of the argon gas at the inlet are the same as those in **Figure 2**. The gas phase temperature was evaluated at the O, A, B and C positions. The maximum gas phase temperature difference from the stage temperature, ΔT, is defined by Equation (1).

$$\Delta T = T_{\text{Diff}} - T_{\text{Stage}} . \tag{1}$$

T_{Stage} is the stage temperature, that is, 350˚C. T_{Diff} is the greatest temperature difference from the T_{Stage} value between the O, A, B and C positions.

The gas phase temperature distribution at the chamber wall temperature of 200˚C is shown in **Figure 3(a)**. The gas phase temperature at the C position is overall lower than those at the O, A and B positions, because of the heat conduction to the cold chamber wall. As shown in **Figure 4(a)**, the gas temperature becomes the lowest value at the height near 80 mm above the stage. At the O, A, B and C positions, the lowest gas phase temperature is 340˚C, 325˚C, 315˚C and 300˚C, respectively. The ΔT value is −50˚C when the chamber wall temperature is 200˚C.

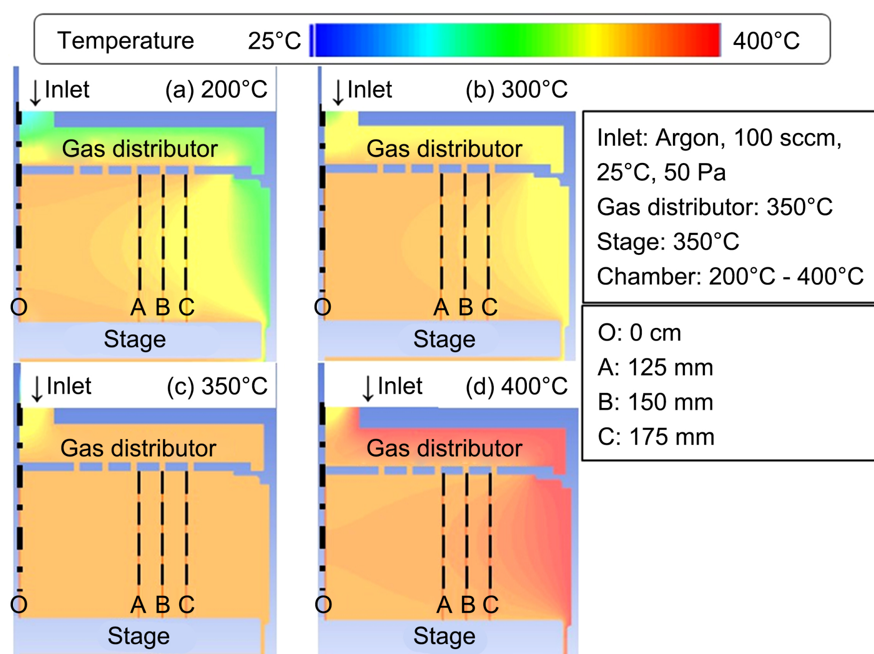

Figure 3. Gas temperature at chamber wall temperature of (a) 200˚C, (b) 300˚C, (c) 350˚C and (d) 400˚C.

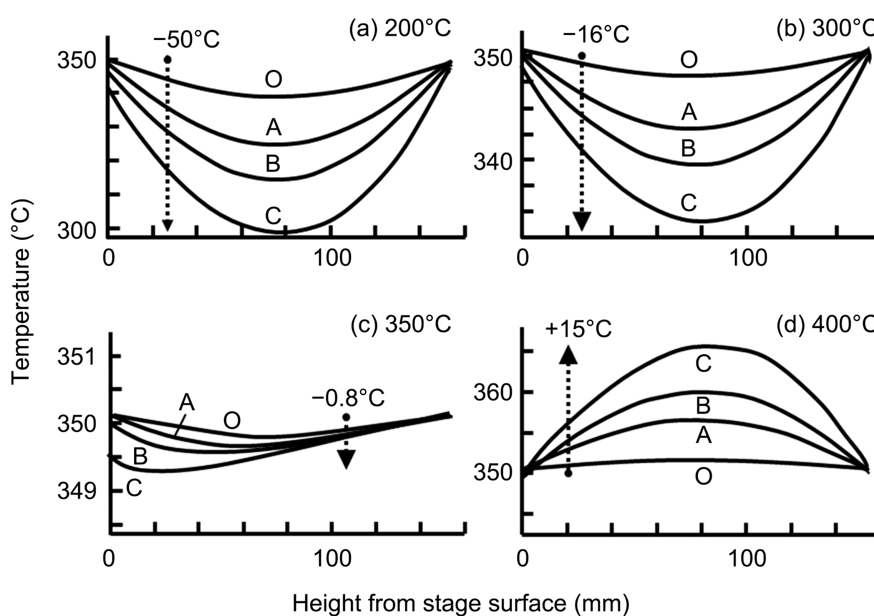

Figure 4. Gas temperature profile at chamber wall temperature of (a) 200˚C, (b) 300˚C, (c) 350˚C and (d) 400˚C.

Figure 3(b) and Figure 4(b) show the temperature distribution when the chamber wall has the temperature of 300˚C. Because the temperature differences between the stage, the gas distributor and the chamber wall are less than those in Figure 3(a) and Figure 4(a), the decrease in the gas phase temperature becomes less than that in Figure 3(a) and Figure 4(a). The ΔT value is −16˚C, as shown in Figure 4(b).

When the chamber wall temperature is 350˚C, the gas phase temperature is overall around 350˚C, as shown in **Figure 3(c)** and **Figure 4(c)**. The ΔT value is significantly low, such as −0.8˚C, as shown in **Figure 4(c)**.

When the chamber wall temperature is 400˚C, the gas phase between the stage and the gas distributor is heated to the temperatures higher than 350˚C by the hot chamber wall, as shown in **Figure 3(d)** and **Figure 4(d)**. The temperature increase is about 1˚C at the O position. The temperature difference from that of the stage increases with approaching the chamber wall. The highest temperature is 365˚C at the C position. The ΔT value in **Figure 3(d)** is +15˚C, as shown in **Figure 4(d)**.

Figure 5 shows the relationship between the ΔT value and the chamber wall temperature. As shown in this figure, the ΔT value monotonously increases with the increasing chamber wall temperature. Based on this figure, the ΔT value is recognized to have a linear relationship with the chamber wall temperature when the heat transport is caused by the thermal conduction without gas recirculation, as shown in **Figure 2**.

While the temperatures of all parts in the reactor should be the same for achieving a uniform temperature distribution, **Figure 5** is expected to be useful to finely adjust and solve the temperature gradient which is unintentionally formed due to any unavoidable reasons.

3.2. Temperature with Gas Recirculation

The gas flow and the temperature were next studied when the gas recirculation exists in the chamber. **Figure 6** shows the gas flow and the velocity distribution at the gas pressures of (a) 500 Pa, (b) 1000 Pa, (c) 2000 Pa and (d) 5000 Pa. The chamber wall temperature is set to 200˚C so that the influence of the gas pressure on the gas phase temperature is clearly recognized.

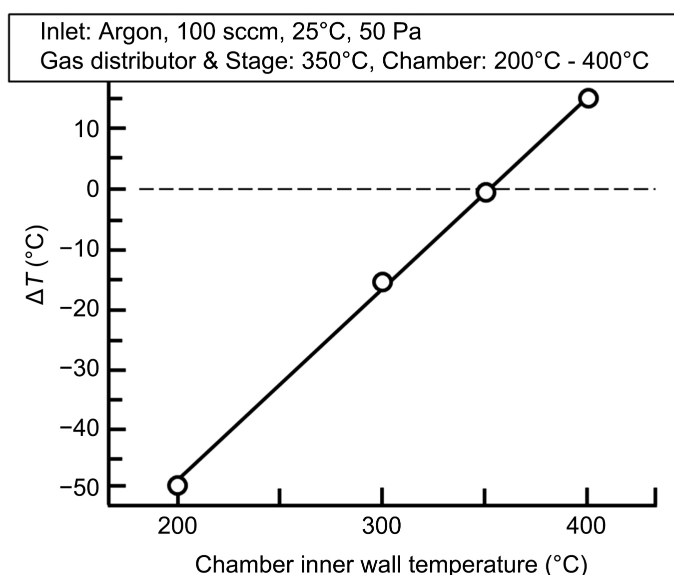

Figure 5. The ΔT value at various chamber wall temperatures.

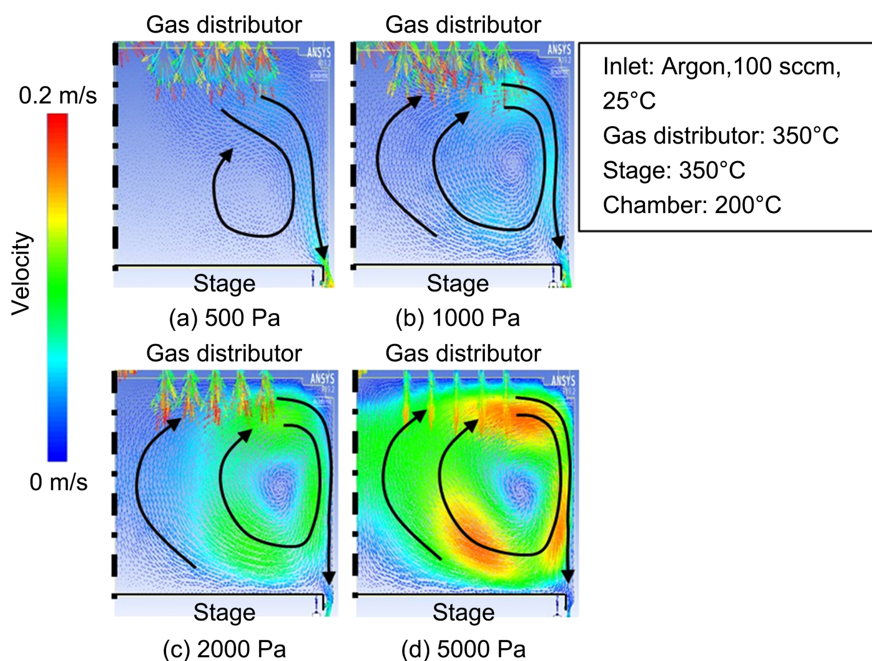

Figure 6. Gas flow and velocity at gas pressure of (a) 500 Pa, (b) 1000 Pa, (c) 2000 Pa and (d) 5000 Pa.

At the gas pressure of 500 Pa, as shown in Figure 6(a), the gas overall flows are downward through the gas distributor. In the region near the stage surface, there is a small and significantly slow gas recirculation as indicated by the arrows.

The gas recirculation is enhanced by the increasing gas pressure. At 1000 Pa, as shown in Figure 6(b), the dimension of the gas recirculation is enhanced to reach the center region of the stage, at which the gas velocity is even significantly low. Figure 6(c) and Figure 6(d) show that the gas recirculation has the gas velocity of about 0.1 m/s and about 0.2 m/s at 2000 Pa and 5000 Pa, respectively, in the wide gas region from the stage to the gas distributor. Overall, the gas velocity and the dimension of the gas recirculation increase with the increasing gas phase pressure.

The gas recirculation shown in Figure 6 influences the gas phase temperature, as showed in Figure 7 and Figure 8. Figure 7(a) and Figure 8(a) show that the mid height at the A, B and C positions has the lowest temperature, similar to those in Figure 3(a), Figure 4(a), Figure 7(b) and Figure 8(b). In contrast, as shown in Figure 7(c) and Figure 7(d), the gas cooled by the cold chamber wall flows to the stage, following the enhanced recirculation indicated by Figure 6(c) and Figure 6(d), the gas phase in the lower half of the chamber is colder than the upper half region.

As shown in Figure 8(a), Figure 8(b) and Figure 8(c), the temperature decreases caused at the O, A, B and C positions are similar at the gas phase pressures between 500 Pa and 2000 Pa. The ΔT values are between −47˚C and −49˚C. While the height showing the lowest temperature at the C position

slightly shifted to near 60 mm at 2000 Pa, the overall temperature profiles are considered to be unchanged at the gas phase pressure less than 2000 Pa; the gas recirculation produced at 500 - 2000 Pa does not significantly worsen the gas temperature uniformity. In contrast, at 5000 Pa, the enhanced gas recirculation indicated by Figure 6(d) significantly takes the heat away from the center region of the gas phase to decrease the gas phase temperature. At the C position, the ΔT value is −76˚C at 5000 Pa.

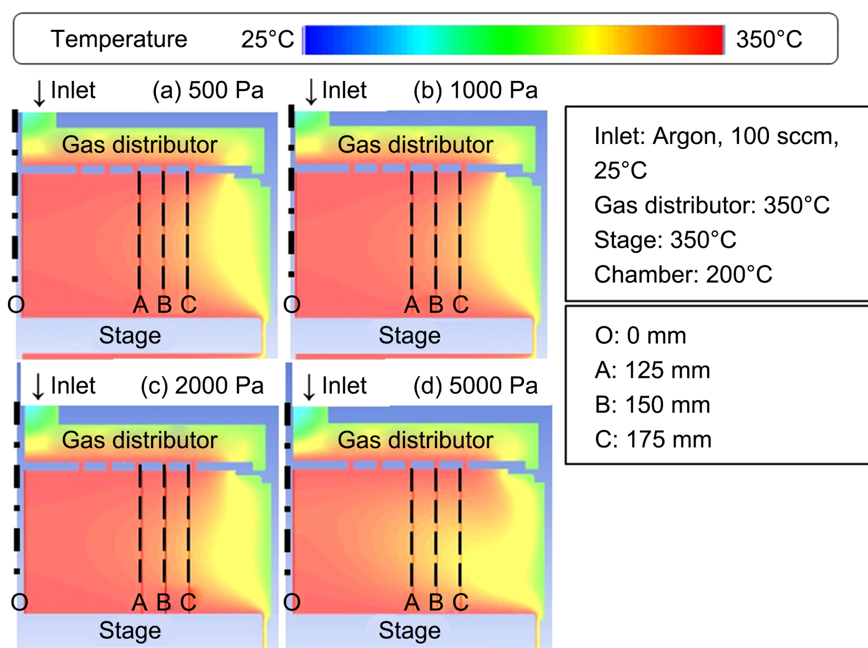

Figure 7. Gas temperature at gas pressure of (a) 500 Pa, (b) 1000 Pa, (c) 2000 Pa and (d) 5000 Pa.

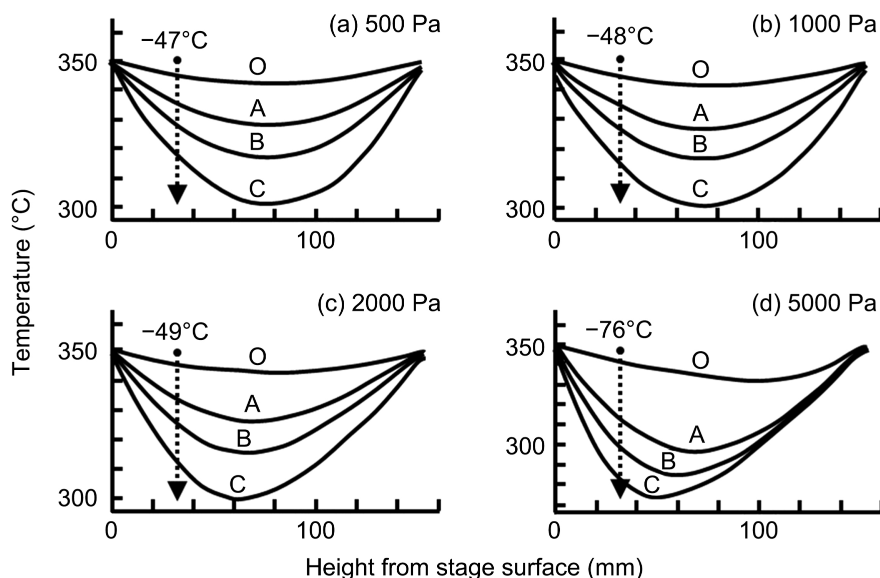

Figure 8. Gas temperature profile at gas pressure of (a) 500 Pa, (b) 1000 Pa, (c) 2000 Pa and (d) 5000 Pa.

The ΔT values are −47˚C, −48˚C, −49˚C and −76˚C at the pressures of 500, 1000, 2000 and 5000 Pa, respectively, as shown in **Figure 9**. This figure shows that the influence of the gas recirculation on the temperature distribution is slight at a pressure lower than 2000 Pa when the gas flow rate is 100 sccm. Because the influence of the gas recirculation may become significant at the gas pressures higher than some specific value, the relationship between the gas pressure and the formed film quality should be carefully evaluated.

3.3. Equation and Contour Diagram

The gas phase temperature distributions were further evaluated for various parameters, such as the stage temperature, T_{Stage} (˚C), the gas distributor temperature, T_{GD} (˚C), the chamber wall temperature, T_{CW} (˚C), the gas pressure, P (Pa), and the gas flow rate, F (sccm). The temperature of the gas inlet was 25˚C. Next, the gas phase temperature uniformity at the i position, X_i, (%) was evaluated by Equation (2) using the maximum and minimum temperature, $T_{\text{Max},i}$ (˚C) and $T_{\text{Min},i}$ (˚C), respectively.

$$X_i(\%) = 100 \times \left(T_{\text{Max},i} - T_{\text{Min},i}\right) \div \left(T_{\text{Max},i} + T_{\text{Min},i}\right). \tag{2}$$

The influences of the various parameters on the X_{O}, X_{A}, X_{B} and X_{C} values are expressed by Equations (3)-(6) which are obtained by the least squares method.

At the O position:

$$X_{\text{O}}(\%) = -0.324T_{\text{GD}} + 4.20\times10^{-4}T_{\text{GD}}^2 - 7.78\times10^{-3}T_{\text{CW}} - 2.49\times10^{-4}P + 4.28\times10^{-3}F + 65.7. \tag{3}$$

At the A position:

$$X_{\text{A}}(\%) = -0.295T_{\text{GD}} + 3.70\times10^{-4}T_{\text{GD}}^2 - 1.38\times10^{-2}T_{\text{CW}} + 4.67\times10^{-4}P + 3.27\times10^{-3}F + 63.9. \tag{4}$$

At the B position:

$$X_{\text{B}}(\%) = -0.262T_{\text{GD}} + 3.17\times10^{-4}T_{\text{GD}}^2 - 1.96\times10^{-2}T_{\text{CW}} + 6.70\times10^{-4}P + 2.27\times10^{-3}F + 61.0. \tag{5}$$

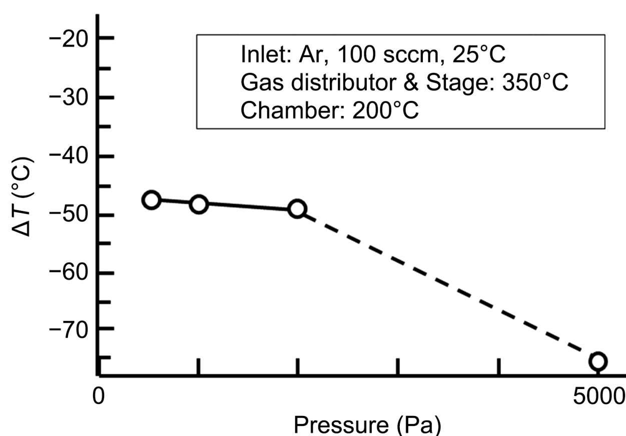

Figure 9. The ΔT value at various gas pressures.

At the C position:

$$X_C(\%) = -0.211T_{GD} + 2.35\times10^{-4}T_{GD}^2 - 3.05\times10^{-2}T_{CW} + 7.32\times10^{-4}P + 1.35\times10^{-3}F + 57.6. \tag{6}$$

Utilizing Equations (3)-(6), the temperature uniformities, X_i, at the O, A, B and C positions are drawn as contour diagrams, as shown in **Figure 10**. In **Figure 10**, the temperatures of the gas distributor, chamber wall and stage are fixed at 350˚C. **Figure 10(A)** shows that the X_O value is overall less than 3%. As shown in **Figure 10(A)**, **Figure 10(B)** and **Figure 10(C)**, the X_A, X_B and X_C values increase with the increasing gas pressure and the increasing gas flow rate, while the trends of the A, B and C positions are slightly different from each other.

Based on **Figure 10**, the gas phase temperature uniformity can be adjusted by the process parameters, such as the gas flow rate and the gas pressure. When the gas phase temperature uniformity is less than 3%, the gas pressure and the gas flow rate are adjusted to those in the left bottom region of the 3% line.

3.4. Gas Residence Time

The gas residence time, t_{RT} (s), was obtained, as shown in **Figure 11**, by tracing the virtual particles from the inlet to the exhaust in the reactor utilizing the Fluent software. For this calculation, the temperatures of the gas distributor, chamber wall and stage are fixed at 350˚C.

As shown in **Figure 11(a)**, the maximum gas residence time, $t_{RT,Max}$ (s), at 1000 Pa decreases with the increasing gas flow rate, because of the increase in the gas velocity over the gas phase in the reactor. While the $t_{RT,Max}$ value is about 500 s at 50 sccm, it decreases to 400 s at the gas flow rate of 100 sccm. At 500 sccm, the $t_{RT,Max}$ value becomes significantly short to achieve the quick removal of the precursor and the byproducts.

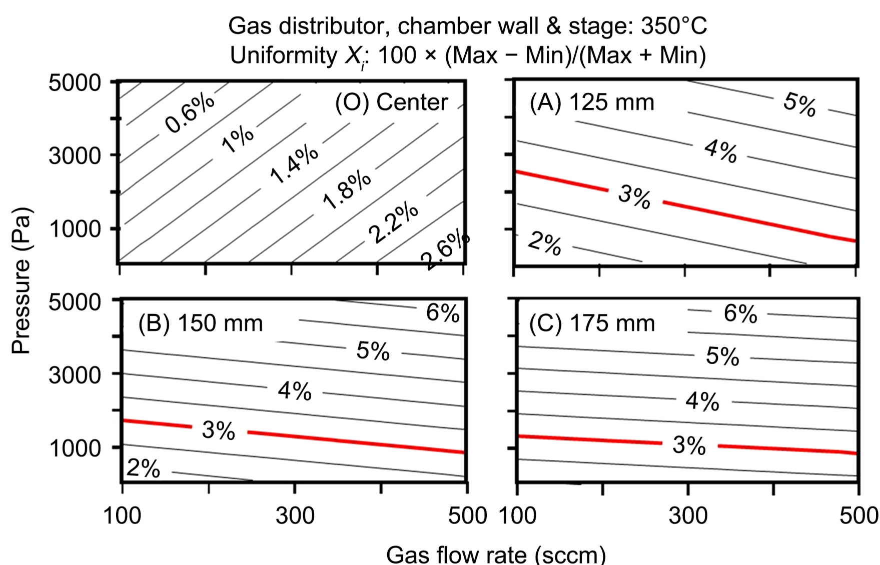

Figure 10. Contour diagrams of temperature uniformity (%) at (O) 0 mm, (A) 125 mm, (B) 150 mm and (C) 175 mm, from center.

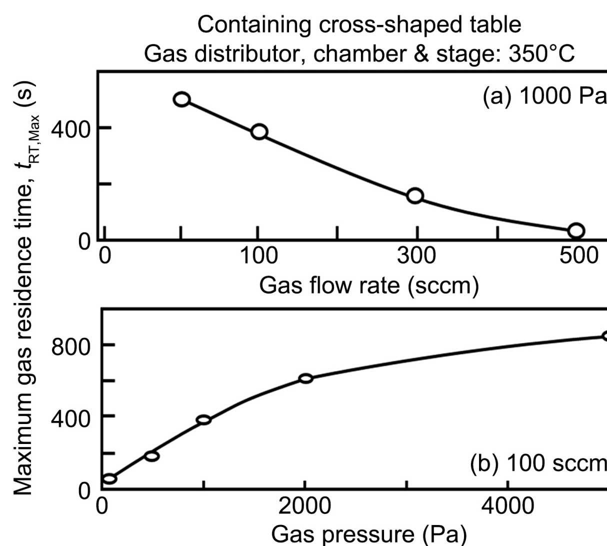

Figure 11. Maximum residence time along with (a) gas flow rate and (b) gas pressure.

When the gas flow rate is fixed, the high gas pressure makes the $t_{RT,Max}$ value long, as shown in **Figure 11(b)**, due to the significant gas recirculation, as shown in **Figure 6(d)**. For preparing the $t_{RT,Max}$ value shorter than 400 s, the gas pressure should be lower than 1000 Pa at the gas flow rate of 100 sccm.

Accounting for the X_i and $t_{RT,Max}$ values, shown in **Figure 10** and **Figure 11**, respectively, the process parameters can be determined. By adjusting the parameter values with evaluating the $t_{RT,Max}$ value, the ALD process is expected to become fast.

While the cross-shaped table, shown in **Figure 1(b)**, is placed on the stage, its influence on the maximum gas residence time is considered to be negligible. When many tables are stacked on the stage in order to increase the number of samples, the gas residence time should be evaluated for avoiding any unexpected gas stagnation behind the table.

3.5. Practical Design Method

A practical design method using the CFD for the ALD gas conditions is summarized as shown in **Figure 12**. It consists of the four steps. 1) At the low gas pressure producing no gas recirculation, the ΔT values are obtained taking into account the various parameters, such as the temperatures of the sample stage, the gas distributor and the chamber wall. 2) The influence of the gas pressure on the ΔT value is studied taking into account the existence of the gas recirculation. 3) The contour diagrams of the temperature uniformity are obtained for determining the applicable combinations of the process conditions utilizing the temperature uniformity equations consisting of various parameters. 4) The relationships of the maximum gas residence time with the gas flow rate and the gas pressure are obtained for determining the range of the process conditions for achieving a fast process.

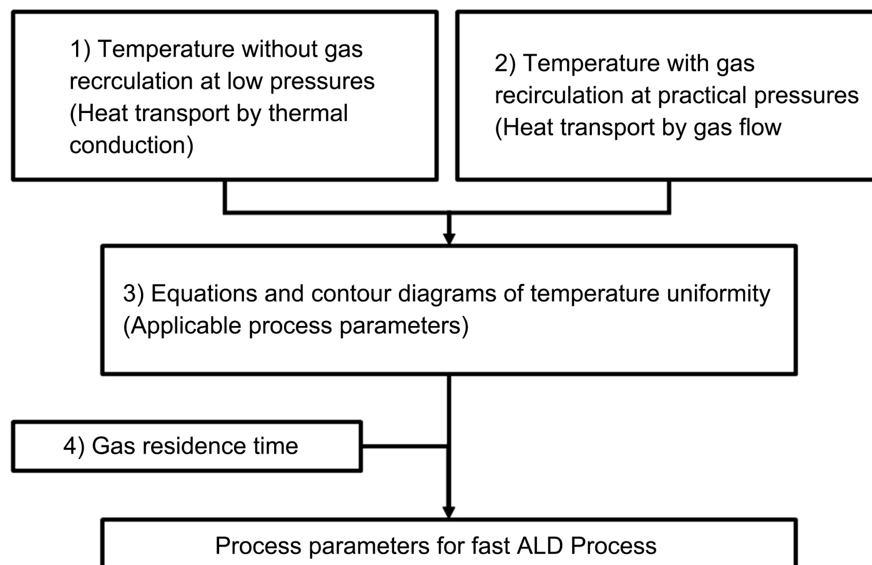

Figure 12. Practical design method of gas conditions for ALD.

The evaluation of the gas flow and the temperature in the gas phase without the recirculation shows the potential capability for temperature uniformity in the reactor. By adding the analysis taking into account the gas recirculation and the gas residence time, the applicable ranges of the various parameters are determined without degrading the temperature uniformity and the processing time.

4. Conclusions

The temperature distribution and the gas residence time in the ALD reactor were evaluated using the CFD. The gas temperature range, that is, the difference between the highest and the lowest gas temperature, linearly increases with the increasing chamber wall temperature when there is no gas recirculation. The significant gas recirculation produced by the increasing gas pressure was shown to make the gas temperature uniformity worse. Next, the temperature uniformities (%) are expressed as contour diagrams based on the equations consisting of the various process parameters. Additionally, the maximum gas residence time is shown to decrease and increase with the increasing gas flow rate and the increasing gas pressure, respectively.

Based on these results, the practical design method of the ALD conditions was studied. After the influences of the thermal conduction and the gas flow were individually evaluated, the range of the practical parameters was visualized utilizing the equation and the contour diagrams of the temperature uniformity. By adding the maximum gas residence time information, the parameters, such as the gas flow rate and the gas pressure, were adjusted. The diagrams and the method in this study are expected to be useful for achieving a fast ALD process.

Conflicts of Interest

The authors declare no conflicts of interest regarding the publication of this paper.

References

[1] Oviroh, P.O., Akbarzadeh, R., Pan, D., Coetzee, R.A.M. and Jen, T. (2019) New Development of Atomic Layer Deposition: Processes, Methods and Applications. *Science and Technology of Advanced Materials*, **20**, 465-496. https://doi.org/10.1080/14686996.2019.1599694

[2] Ruzyllo, J. (2020) Guide to Semiconductor Engineering. *World Scientific*, Singapore. https://doi.org/10.1142/11706

[3] Suntola, T. (1992) Atomic Layer Epitaxy. *Thin Solid Films*, **216**, 84-89. https://doi.org/10.1016/0040-6090(92)90874-B

[4] Puurunen, R.L. (2014) A Short History of Atomic Layer Deposition: Tuomo Suntola's Atomic Layer Epitaxy. *Chemical Vapor Deposition*, **20**, 332-344. https://doi.org/10.1002/cvde.201402012

[5] Yabu, H. (2018) Fabrication of Honeycomb Films by the Breath Figure Technique and Their Applications. *Science and Technology of Advanced Materials*, **19**, 802-822. https://doi.org/10.1080/14686996.2018.1528478

[6] Fogler, H.S. (2011) Essentials of Chemical Reaction Engineering. Pearson, Boston.

[7] Pan, D., Ma, L. and Xie, Y. (2015) On the Physical and Chemical Details of Alumina Atomic Layer Deposition: A Combined Experimental and Numerical Approach. *Journal of Vacuum Science & Technology A*, **33**, Article ID: 021511. https://doi.org/10.1116/1.4905726

[8] Shaeri, M.R., Jen, T.C. and Yuan, C.Y. (2014) Improving Atomic Layer Deposition Process through Reactor Scale Simulation. *International Journal of Heat and Mass Transfer*, **78**, 1243-1253. https://doi.org/10.1016/j.ijheatmasstransfer.2014.07.079

[9] Pan, D., Ma, L., Xie, Y., Wang, F., Jen, T. and Yuan, C. (2015) Experimental and Numerical Investigations into the Transient Multi-Wafer Batch Atomic Layer Deposition Process with Vertical and Horizontal Wafer Arrangements. *International Journal of Heat and Mass Transfer*, **91**, 416-427. https://doi.org/10.1016/j.ijheatmasstransfer.2015.07.123

[10] Shaeri, M.R., Jen, T.C. and Yuan, C.Y. (2015) Reactor Scale Simulation of an Atomic Layer Deposition Process. *Chemical Engineering Research and Design*, **94**, 584-593. https://doi.org/10.1016/j.cherd.2014.09.019

[11] Suh, S., Park, S., Lim, H., Choi, Y., Hwang, C. and Kim, H. (2012) Investigation on Spatially Separated Atomic Layer Deposition by Gas Flow Simulation and Depositing Al_2O_3 Films. *Journal of Vacuum Science & Technology A*, **30**, Article ID: 051504. https://doi.org/10.1116/1.4737123

[12] Sarakikya, H., Mashingo, P. and Kilonzo, F. (2021) Design and Computational Fluid Dynamics Modeling for a Municipal Solid Waste Incineration Process. *Open Journal of Fluid Dynamics*, **11**, 177-191. https://doi.org/10.4236/ojfd.2021.114011